INORGANIC CHEMISTRY
FRONTIERS

RESEARCH ARTICLE

View Article Online
View Journal | View Issue

Check for updates

Cite this: *Inorg. Chem. Front.*, 2018, **5**, 29

# Encapsulating surface-clean metal nanoparticles inside metal–organic frameworks for enhanced catalysis using a novel γ-ray radiation approach†

Zhen Zhang,[a] Xiaoling Cui,[a] Wei Yuan,[a] Qihao Yang,[b] Huarong Liu, *[a] Hangxun Xu *[a] and Hai-Long Jiang *[b]

Received 17th September 2017,
Accepted 14th October 2017

DOI: 10.1039/c7qi00577f

rsc.li/frontiers-inorganic

A facile and efficient γ-radiation strategy has been developed to incorporate surface-clean metal nanoparticles (NPs) into UiO-66-$NH_2$ in the absence of stabilizing agents and additional reductants. This approach is enabled by metal ion reduction with active $e^-_{aq}$ and H• species derived from water radiolysis. As a result, highly dispersed Pd NPs with narrow size distribution were generated and evenly dispersed in UiO-66-$NH_2$. More importantly, the radiation-reduced Pd NPs exhibit significantly enhanced catalytic activity and stability in olefin hydrogenation. Meanwhile, they are also highly active in the catalytic reduction of 4-nitrophenol to 4-aminophenol. Furthermore, the proposed radiation methodology could be successfully extended to prepare other metal NPs such as Au and Pt. Considering that γ-ray radiation is widely used in industry, this study provides a potentially scalable approach to incorporate metallic nanomaterials into metal–organic frameworks with improved catalytic performance.

Published on 16 October 2017. Downloaded on 17/01/2018 00:24:45.

## 1. Introduction

As an emerging class of highly porous crystalline materials, metal–organic frameworks (MOFs) assembled from inorganic metal-containing nodes and organic ligands have attracted enormous interest in recent years.[1–5] MOFs have been extensively investigated for a wide range of applications in separation,[6–8] gas storage,[9–11] chemical sensing,[12–14] and drug delivery.[15,16] Particularly, MOFs also hold great potential for heterogeneous catalysis due to their unique porous structures which make MOFs suitable for incorporating various catalytically active species into their well-organized pores.[17–21] This unique capability not only enables MOFs to possess enhanced catalytic performance but also broadens their applications in chemical reactions which are not feasible by individual components. One of the most promising catalytic species that are intensively explored is metal nanoparticles (MNPs) due to their important applications in heterogeneous catalysis. Therefore, the integration of MNPs with MOFs for enhanced or potentially unprecedented catalytic performance has become an important research topic.

In light of the significance of rational combination of MNPs with MOFs, various methodologies have been developed to incorporate MNPs into MOFs *via* either inclusion of metallic precursors followed by controlled decomposition/reduction[22–24] or assembling MOFs with pre-formed MNPs.[25–30] For example, Xu *et al.* developed a novel "double solvents" method to immobilize ultrafine Pt nanoparticles inside the pores of MIL-101 without the formation of Pt nanoparticles on the external surface of the frameworks.[31] Huang *et al.* used UiO-66-$NH_2$ as the scaffold to synthesize nanoparticles that were confined in MOF cavities. The amine groups on terephthalic acid linkers in UiO-66-$NH_2$ could provide coordination sites for metal ions.[32,33] Li *et al.* developed a novel and efficient kinetically modulated protocol for the controlled embedding of "clean" Pt clusters into MOFs.[34] Rational control over the size and spatial distribution of Pt clusters is achieved by using acetic acid as a MOF-formation modulator to decrease the growth rate of MOFs and using $H_2$ as an assistant reductant to promote the formation rate of Pt, respectively. We recently obtained hollow ZIF-8 nanospheres with controllable shell thicknesses through a facile emulsion-based interfacial synthesis.[35] We further showed that Pd nano-

[a]*CAS Key Laboratory of Soft Matter Chemistry, Department of Polymer Science and Engineering, University of Science and Technology of China, Hefei, Anhui 230026, P. R. China. E-mail: hrliu@ustc.edu.cn, hxu@ustc.edu.cn*
[b]*CAS Key Laboratory of Soft Matter Chemistry, Hefei National Laboratory for Physical Sciences at the Microscale, Department of Chemistry, University of Science and Technology of China, Hefei, Anhui 230026, P. R. China. E-mail: jianglab@ustc.edu.cn*

†Electronic supplementary information (ESI) available: Additional table of experimental conditions, PXRD, TEM, XPS, $^1$H NMR, nitrogen adsorption and desorption isotherms, UV-Vis absorption spectra characterization results. See DOI: 10.1039/c7qi00577f

Published on 16 October 2017. Downloaded on 17/01/2018 00:24:45.

cubes can be easily encapsulated into the cavities of hollow MOF nanospheres to form Pd@ZIF-8 hybrid nanospheres by introducing Pd nanocubes to the aqueous phase during the emulsification process.

Despite remarkable progress in the synthesis of MNP/MOF composites, these synthetic methods are generally tedious and inefficient. For instance, in the case of assembling MOFs with pre-formed MNPs, capping agents are indispensable to restrict the aggregation of MNPs and facilitate the growth of MOFs around the MNPs.[36–39] However, the capping agents are often difficult to be completely removed, inevitably leading to reduced catalytic activity.[40] Meanwhile, the other synthetic approach, which involves impregnation of metallic precursors followed by reduction, requires the use of dangerous and environment unfriendly reducing agents such as $NaBH_4$ (violent), $N_2H_4{\cdot}H_2O$ (toxic), or $H_2$ (flammable). Although microwave-assisted reduction,[41] UV light radiation,[30] and controlled decomposition methods[42] have been applied as alternative approaches in the synthesis of MNP/MOF composites, these approaches are neither applicable to diverse precursors nor suitable for scalable production. Therefore, the development of a facile, effective, and potentially scalable approach for the incorporation of surface-clean MNPs with narrow size distribution into MOFs without additional stabilizing agents and reductants still remains a great challenge.

The radiation processing technology, as a common and efficient tool, has been widely used in agriculture, industry, medicine, food and environmental protection. Moreover, radiation synthesis through utilizing γ-rays generated from a radioactive source has been proved to be a versatile tool for the controlled synthesis of various inorganic nanomaterials including metals (*e.g.*, Pd, Pt, Au, Ag, and Ni),[43–47] metal oxides (*e.g.*, $Co_3O_4$, $MnO_2$, and $Sb_2O_3$),[48–50] transition-metal hydroxides (*e.g.*, $Co(OH)_2$ and $Ni(OH)_2$),[51–53] and sulfides (*e.g.*, CdS and ZnS).[54–57] This technology shows several distinct advantages such as low energy consumption, free of contaminations from chemical initiators and reductants, and simple production schemes.[58] Therefore, developing the γ-ray radiation method as a viable approach for synthesizing MNP/MOF composites is highly desirable.

Herein, we demonstrate a γ-ray radiation method for the formation of ultrasmall Pd NPs inside MOFs. These Pd NPs were evenly dispersed inside the UiO-66-$NH_2$ with narrow size distribution. Control experiments indicate that the γ-ray radiation method could ensure that all Pd NPs are confined within the MOFs, whereas using $H_2$ or $NaBH_4$ as the reducing agents inevitably leads to the generation of large Pd nanoparticles on the external surface of MOFs. More importantly, Pd NPs prepared using the γ-ray radiation method exhibit significantly enhanced catalytic activity and stability in olefin hydrogenation and catalytic reduction of 4-nitrophenol to 4-aminophenol. We further show that the proposed methodology could be successfully extended to prepare other metal NPs inside the MOFs, implying that the γ-ray radiation technique could be a viable approach for synthesizing various metal NPs inside MOFs with prominent catalytic performance.

## 2. Experimental section

### Materials

Zirconium(IV) chloride (98%), 2-aminoterephthalic acid ($NH_2$-$H_2BDC$) (99%) and 5 wt% Pd/C were purchased from Sigma-Aldrich. Potassium tetrachloropalladate ($K_2PdCl_4$), potassium tetrachloroplatinate ($K_2PtCl_4$), potassium gold chloride ($KAuCl_4$) and 4-nitrophenol (99%) were purchased from Aladdin Reagents. 1-Hexene, trans-stilbene, and tetraphenylethylene were purchased from TCI Chemicals (Japan). Other materials including *N*,*N*′-dimethylformamide (DMF), sodium borohydride ($NaBH_4$), styrene, ethanol, dichloromethane, methanol, isopropyl alcohol, and ethyl acetate were purchased from Sinopharm Chemical Reagent Co., Ltd. All materials were used as received without further purification. Deionized water (18.2 MΩ $cm^{-1}$) from a Milli-Q ultrapure system was used in this study. Nitrogen gas ($N_2$, 99.999%), hydrogen gas ($H_2$, 99.999%), and 5% $H_2$ in Ar were purchased from Nanjing Special Gas Factory Co., Ltd.

### Synthesis of UiO-66-$NH_2$

UiO-66-$NH_2$ was synthesized and purified according to the reported procedure.[59] In a typical experiment, zirconium(IV) chloride (0.40 g) and $NH_2$-$H_2BDC$ (0.31 g) were dissolved in 100 mL of DMF at room temperature, and then 140 μL of deionized water was added. The obtained mixture was sealed and placed in a preheated oven at 120 °C for 24 h. The obtained solid MOFs were washed successively with fresh DMF, dichloromethane, and methanol, and then activated at 150 °C under vacuum for 6 h.

### Radiation synthesis of M@UiO-66-$NH_2$/R

Pd@UiO-66-$NH_2$/R (here 'R' represents radiation reduction) was prepared *via* γ-radiation of UiO-66-$NH_2$ impregnated with $K_2PdCl_4$ solution. To prepare 3.55 wt% Pd@UiO-66-$NH_2$/R, 50 mg of vacuum-dried UiO-66-$NH_2$ was dispersed in 5 mL of aqueous solution containing 8.2 mg (0.025 mmol) of $K_2PdCl_4$ by ultrasonication for 10 min at room temperature. Then, the vial containing the slurry was further stirred at room temperature for 24 h. The impregnated UiO-66-$NH_2$ sample was washed with water three times followed by centrifugation at 8000 rpm for 10 min. Subsequently, the impregnated sample was dispersed in 5 mL water containing 0.2 mL of isopropyl alcohol by ultrasonication for 5 min. After that, the dispersed solution was bubbled with $N_2$ for 30 min to remove $O_2$ and then sealed for irradiation by γ-rays in a field of $1.1 \times 10^{15}$ Bq $^{60}Co$ source at a dose rate of 100 Gy $min^{-1}$ with a total absorbed dose of 18 kGy. The obtained Pd@UiO-66-$NH_2$/R sample was washed with deionized water three times through repeated centrifugation and then dried at 50 °C under vacuum for 6 h. Different absorbed doses and dose rates were applied to study their effects on the reduction of metal ions. Meanwhile, different loading amounts of Pd could be obtained by changing both the concentrations of the impregnating solutions and the absorbed doses as shown in Table S1.†

 This journal is © the Partner Organisations 2018

Published on 16 October 2017. Downloaded on 17/01/2018 00:24:45.

The same procedure was also used to impregnate Pt or Au into UiO-66-$NH_2$ to prepare Pt and Au NPs inside MOFs. In both cases, 5 mL aqueous solution containing 10.4 mg (0.025 mmol) of $K_2PtCl_4$ and 9.5 mg (0.025 mmol) of $KAuCl_4$ was used (Table S1†).

### Synthesis of Pd@UiO-66-$NH_2$/H and Pd@UiO-66-$NH_2$/B

In order to evaluate the catalytic performance of the Pd@UiO-66-$NH_2$/R, Pd@UiO-66-$NH_2$ samples prepared using $H_2$ or $NaBH_4$ as the reducing agents were also synthesized. The impregnation process was identical to the preparation of Pd@UiO-66-$NH_2$/R. For the synthesis of Pd@UiO-66-$NH_2$/H (here 'H' represents $H_2$ reduction), the impregnated UiO-66-$NH_2$ sample was dried at room temperature for 8 h under vacuum after being washed and then reduced in 5% $H_2$/Ar at a flow rate of 50 mL $min^{-1}$ at 200 °C for 3 h. For the synthesis of Pd@UiO-66-$NH_2$/B (here 'B' represents $NaBH_4$ reduction), the impregnated UiO-66-$NH_2$ sample was dispersed into 5 mL of deionized water by ultrasonication for 10 min at room temperature and then 5 mL of $NaBH_4$ aqueous solution (0.075 M) was added dropwise under stirring at 0 °C. This dispersion was further stirred for 3 h at 0 °C. The obtained samples were washed with deionized water three times through centrifugation and then dried at 50 °C under vacuum for 6 h.

### Catalytic hydrogenation of different olefins

The size-selective hydrogenation of olefins was carried out in the batch mode at a pressure of 1 bar static hydrogen with the molar ratio of Pd/olefin of 1 : 100 using 1-hexene, trans-stilbene and tetraphenylethylene as different reactants. In a typical experiment, 9 mg of 3.55 wt% Pd@UiO-66-$NH_2$/R (or 6.4 mg of 5 wt% Pd/C) was dispersed in 10 mL of ethyl acetate solution containing 0.3 mmol of olefin filled in a 20 mL vial. The vial was loaded with an $H_2$ balloon after being purged with $H_2$ several times. The reaction was carried out with a magnetic stirrer at 300 rpm for 24 h. After the reaction, the catalyst was collected by centrifugation and the filtrate (for 1-hexene and trans-stilbene) was analysed and identified by GC. Meanwhile, the catalytic hydrogenation of tetraphenylethylene was monitored using a $^1$H NMR spectrometer.

The catalytic hydrogenation of styrene was selected to evaluate the catalytic performance of different Pd@UiO-66-$NH_2$ samples with different Pd loading amounts. Specifically, a certain amount of catalyst (the molar ratio of Pd to styrene was fixed at 1 : 100) was dispersed in 10 mL of ethanol solution containing 0.3 mmol of styrene. The subsequent procedure is the same as the hydrogenation of 1-hexene. The reaction progress was consecutively monitored by GC.

### Recyclability tests

In order to compare the recyclability of various Pd@UiO-66-$NH_2$, the catalytic hydrogenation of styrene was represented using 5 wt% Pd/C as a contrast. After the previous run is complete, the used catalysts were separated from the reaction mixture by centrifugation, thoroughly washed with deionized water and ethanol three times, respectively, and then heated at 60 °C under vacuum for 6 h. Finally, the recycled catalysts were used to catalyze the hydrogenation of styrene again under the same reaction conditions of the first cycle, and five cycles of the catalytic reaction were tested.

### Catalytic reduction of 4-nitrophenol

The catalytic reactions were carried out under ambient conditions. Typically, 1 mL of 0.3 mM aqueous solution of 4-nitrophenol was added into a quartz cuvette. After that, 1 mL of 0.3 M aqueous solution of fresh $NaBH_4$ and 1 mL of aqueous solution of Pd@UiO-66-$NH_2$ (the molar ratio of Pd to 4-nitrophenol was 1 : 150) were successively added. The reaction was monitored by recording the variations in the optical density of the absorbance maximum at 400 nm on a UV-Vis spectrophotometer.

### Characterization

Transmission electron microscopy (TEM) images were observed on a Hitachi Model H-7650 transmission electron microscope with an accelerating voltage of 100 kV. High resolution TEM (HRTEM) images, scanning transmission electron microscopy (STEM), elemental mapping analyses, and energy dispersive X-ray spectroscopic analysis (EDS) were conducted on a JEM-2100F transmission electron microscope equipped with an EDS detector operating at an accelerating voltage of 200 kV. Powder X-ray diffraction patterns (PXRD) of the product were obtained on a Japan Rigaku D/Max $\gamma_A$ rotation anode X-ray diffractometer equipped with graphite monochromatized Cu Kα radiation ($\lambda$ = 1.54178 Å). The $N_2$ adsorption–desorption measurements were taken at 77.3 K on a Micromeritics ASAP 2020 gas adsorption analyser. Prior to the measurements, samples were degassed at 120 °C for 6 h under vacuum. Surface areas were determined using the Brunauer–Emmett–Teller (BET) method. The pore size distribution was analysed *via* the NLDFT method utilizing the adsorption isotherm. X-ray photoelectron spectroscopy (XPS) analyses were performed on a Thermo ESCALAB 250 X-ray photoelectron spectrometer with Al Kα X-rays as the exciting source. Inductively coupled plasma mass spectra (ICP-MS) were carried out on a Thermo scientific VG Plasma Quad 3. UV-Vis absorption spectra of the samples were recorded on a UV-Vis spectrophotometer (Shimadzu 3600). Catalytic reaction products were analysed and identified by gas chromatography (GC, Agilent 6890). $^1$H NMR spectra were recorded on a Bruker AC-400FT spectrometer (300 MHz).

## 3. Results and discussion

In order to generate metal NPs inside MOFs, various MOFs such as HKUST-1, MIL-101, ZIF-8, and UiO-66-$NH_2$ were synthesized and subjected to high energy γ-ray radiation to assess the stability of MOFs under air atmosphere or water environment. As shown in Fig. S1,† the PXRD patterns clearly indicate that MOFs are stable under γ-ray radiation under different atmospheric conditions, suggesting that they can be used for

Published on 16 October 2017. Downloaded on 17/01/2018 00:24:45.

the *in situ* formation of metal NPs inside MOFs. During water radiolysis, various transient species such as $H^{\bullet}$, $e^{-}_{aq}$, $H_3O^{+}$, and $H_2$ are produced due to the high energy radiation.[60] Among them, highly active $H^{\bullet}$ and $e^{-}_{aq}$ are strong reducing species with redox potentials of $E^{\circ}(H_2O/e^{-}_{aq}) = -2.87\ V_{NHE}$ and $E^{\circ}(H^{+}/H^{\bullet}) = -2.3\ V_{NHE}$, respectively. They could reduce metal ions absorbed on the amino groups of MOFs to the corresponding metal NPs as shown in Scheme 1. However, $OH^{\bullet}$ radicals are strong oxidizing agents with $E^{\circ}(OH^{\bullet}/H_2O) = +2.8\ V_{NHE}$. Thus, $OH^{\bullet}$ scavengers such as isopropyl alcohol should be added to the reaction system prior to irradiation. Consequently, the unique reducing environment is able to reduce different metal ions. Meanwhile, the radiation conditions such as absorbed doses and dose rates could have obvious influence on the formation of metal NPs and their corresponding physicochemical properties. Therefore, the radiation conditions were first screened to determine appropriate conditions for the synthesis of Pd@UiO-66-$NH_2$ as shown in Table S1.† From Fig. S2,† it could be found that Pd NPs were uniformly dispersed in UiO-66-$NH_2$ with absorbed doses of 6 kGy or 18 kGy at a dose rate of 100 Gy $min^{-1}$. In contrast, increasing the absorbed dose (36 kGy at a dose rate of 100 Gy $min^{-1}$) or reducing the dose rate (25 Gy $min^{-1}$ with the absorbed dose of 18 kGy) could generate large Pd nanoparticles (Fig. S2c and S2d†).

Apparently, increasing the dose rate could lead to a higher concentration of reducing species from water radiolysis, causing rapid reduction of metal ions and thus creating a large number of nucleated $Pd^0$ seeds which is beneficial for the formation of uniform Pd NPs. On the other hand, increasing absorbed doses could reduce more metal ions, resulting in a large number of Pd NPs encapsulated in UiO-66-$NH_2$ (Table S2†); however, excessively absorbed doses inevitably produce Pd particles with large sizes as shown in Fig. S2c.† Therefore, considering both the dose rates and absorbed doses, Pd@UiO-66-$NH_2$/R was prepared at a dose rate of 100 Gy $min^{-1}$ with the absorbed dose of 18 kGy.

In addition, the amount of $K_2PdCl_4$ impregnated in UiO-66-$NH_2$ is another important parameter for the synthesis of Pd NPs inside MOFs. From Fig. S3 and Table S3,† it can be seen that when the concentration of $K_2PdCl_4$ increased from 0.002 M to 0.005 M then to 0.010 M, the diameter of Pd NPs increases from 1.7 nm to 1.9 nm then to 3.7 nm. Accordingly, the amount of Pd inside MOFs increases from 1.52 wt% to 3.55 wt% and then to 6.90 wt% as determined from ICP-MS. Therefore, the concentration of $K_2PdCl_4$ was maintained below 0.005 M during the synthesis to obtain ultrasmall Pd NPs. As shown in Fig. 1a, the high-resolution TEM image clearly reveals the formation of uniform Pd NPs inside UiO-66-$NH_2$. Meanwhile, the high-angle annular dark-field scanning TEM (HAADF-STEM) image further confirms the uniformity of the Pd NPs in the UiO-66-$NH_2$ framework (Fig. 1b). Moreover, the corresponding elemental mapping results further verify that Pd NPs are evenly distributed inside the MOFs. Due to a similar contrast of Zr-oxo clusters in UiO-66-$NH_2$ to that of Pd NPs upon exposure to an electron beam, there are probably some indiscernible Pd NPs with less than 1 nm in diameter in the UiO-66-$NH_2$ framework. Although a small fraction of Pd NPs are larger than the pore size of UiO-66-$NH_2$ (~12 Å),[61] the pore structure could offer spatial restriction to Pd NPs to some extent in accordance with previous reports.[29,62]

Fig. 2a shows the PXRD patterns of Pd@UiO-66-$NH_2$/R catalysts along with the simulated UiO-66-$NH_2$. Obviously, the diffraction patterns of Pd@UiO-66-$NH_2$/R catalysts are identical to the simulated structure, indicating that the crystal structure of UiO-66-$NH_2$ was well retained. The characteristic peak of Pd (111) at $2\theta \approx 40.1°$ was absent in the PXRD patterns, which could presumably be related to the low content and the small size of generated Pd NPs.[29] The nitrogen sorption isotherms indicated that UiO-66-$NH_2$ exhibited a BET surface area about 1126 $m^2\ g^{-1}$ (Fig. 2b). After immobilizing Pd NPs, the specific surface area decreased significantly to 782 and 750 $m^2\ g^{-1}$ for 1.52 and 3.55 wt% Pd@UiO-66-$NH_2$/R, respectively. Meanwhile, the pore volume of Pd@UiO-66-$NH_2$/R also decreased compared to UiO-66-$NH_2$ (Table S4†), indicating that the cavities were occupied by the formed Pd NPs.

To evaluate the advantages of the proposed γ-ray radiation strategy, other reducing methods were also employed to

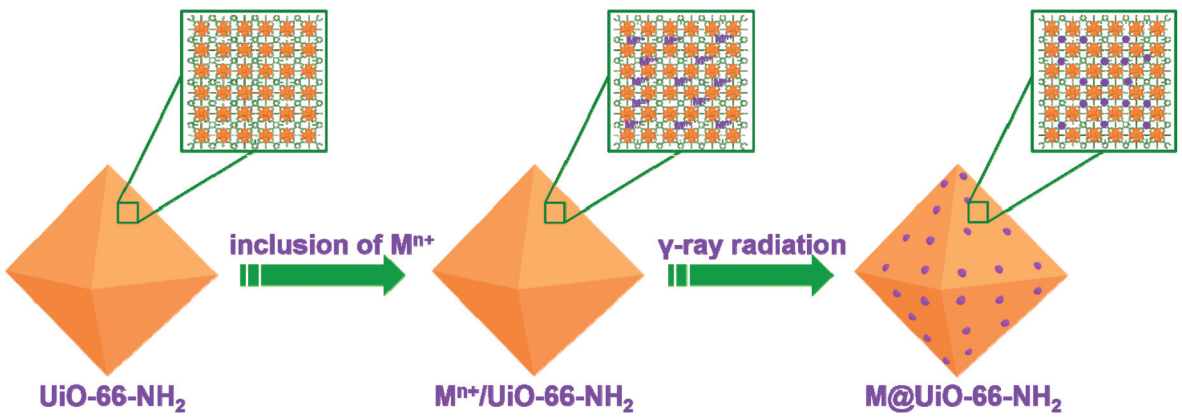


**Scheme 1** Schematic illustration of the synthetic route for the formation of metal nanoparticles inside UiO-66-$NH_2$ *via* the γ-ray radiation approach.

 This journal is © the Partner Organisations 2018

Published on 16 October 2017. Downloaded on 17/01/2018 00:24:45.

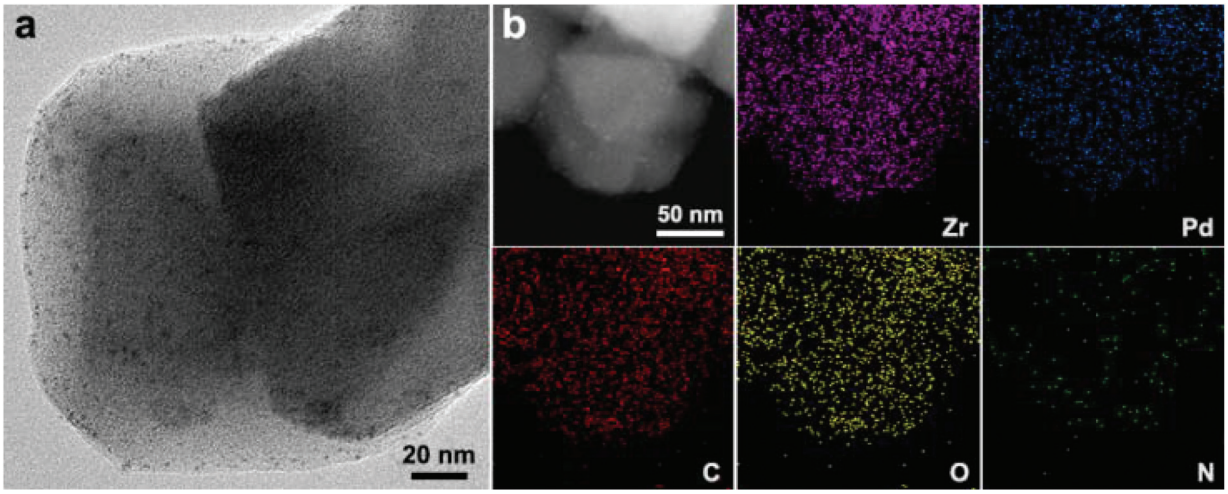


Fig. 1 (a) TEM image of Pd@UiO-66-$NH_2$/R (3.55 wt% Pd). (b) HAADF-STEM image and the corresponding elemental mapping images of Zr, Pd, C, O, and N.

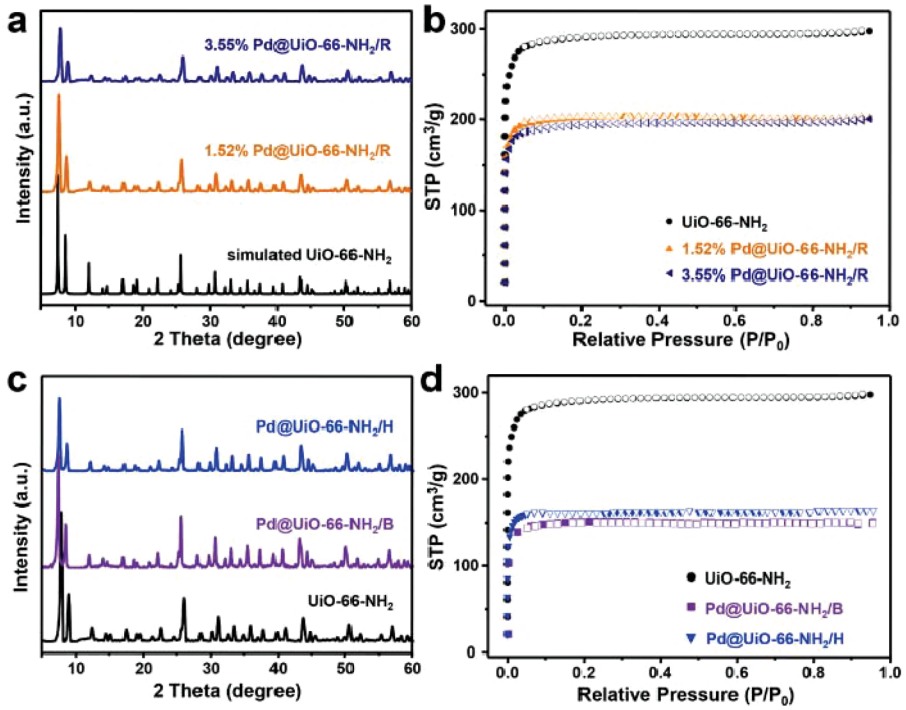


Fig. 2 (a) PXRD patterns and (b) nitrogen adsorption and desorption isotherms of UiO-66-$NH_2$, Pd@UiO-66-$NH_2$/R (1.52 and 3.55 wt% Pd). (c) PXRD patterns and (d) nitrogen adsorption and desorption isotherms of UiO-66-$NH_2$, Pd@UiO-66-$NH_2$/B, and Pd@UiO-66-$NH_2$/H.

prepare Pd@UiO-66-$NH_2$ catalysts for comparison (see the Experimental section for details). The PXRD patterns indicated the crystallinity of UiO-66-$NH_2$ still maintained in Pd@UiO-66-$NH_2$/H and Pd@UiO-66-$NH_2$/B (Fig. 2c). The measured BET surface areas of Pd@UiO-66-$NH_2$/H and Pd@UiO-66-$NH_2$/B were 608 and 585 $m^2\ g^{-1}$, respectively (Fig. 2d). These values were much lower than that of the Pd@UiO-66-$NH_2$/R catalyst even with the higher Pd loading amount (Tables S3 and S4†). Moreover, the pore volume of Pd@UiO-66-$NH_2$/R was larger than those of Pd@UiO-66-$NH_2$/H and Pd@UiO-66-$NH_2$/B. Further microstructure examination using TEM (Fig. S4†) indicated that large Pd nanoparticles were formed both in Pd@UiO-66-$NH_2$/H and Pd@UiO-66-$NH_2$/B with heterogeneous distribution. These results clearly indicate that γ-ray radiation is a novel approach to achieve Pd NPs with uniform distribution in porous frameworks.

XPS was performed to examine the composition and the valence state of the as-synthesized Pd NPs. As shown in

Published on 16 October 2017. Downloaded on 17/01/2018 00:24:45.

Fig. S5,† it can be clearly seen that the $3d_{5/2}$ and $3d_{3/2}$ peaks of $Pd^0$ appear at 338.1 and 343.5 eV, respectively. Both peaks slightly shift to the higher energy due to the interaction between Pd and Zr.[63] It is noteworthy that there is an additional small peak at *ca.* 341.3 eV in the Pd@UiO-66-$NH_2$/H and Pd@UiO-66-$NH_2$/B. This peak was probably ascribed to the absorbed $Pd^{2+}$ by the amine groups in UiO-66-$NH_2$ during impregnation and/or the oxidized Pd NPs distributed on the outer surface of MOFs. They were not only difficult to be removed by repeated washing but also difficult to be completely reduced by $H_2$ or $NaBH_4$ due to the limited diffusion of $H_2$ or $NaBH_4$ into the porous MOFs. In sharp contrast, the $Pd^{2+}$ peak could not be observed in Pd@UiO-66-$NH_2$/R, suggesting that γ-ray radiation is very efficient to reduce $Pd^{2+}$ into $Pd^0$ with high penetration capability. Moreover, the Pd content of 3.55 wt% Pd@UiO-66-$NH_2$/R measured from the XPS analysis was lower than that found in Pd@UiO-66-$NH_2$/H and Pd@UiO-66-$NH_2$/B, although ICP-MS measurements revealed that Pd@UiO-66-$NH_2$/R possessed much higher Pd content (Table S3†). This observation clearly confirms that γ-ray radiation could reduce most of the $Pd^{2+}$ inside the UiO-66-$NH_2$ frameworks through using the *in situ* generated $H^{\bullet}$ and $e^-_{aq}$, whereas other methods only reduce $Pd^{2+}$ located near the surface region of the MOFs due to the limited diffusion of $H_2$ or $NaBH_4$. This observation is also consistent with the colour variance in the obtained Pd@UiO-66-$NH_2$ samples (Fig. S6†). Furthermore, although the impregnation condition was the same for all samples and almost all $Pd^{2+}$ (99.99%, calculated by ICP-MS) were absorbed by UiO-66-$NH_2$, the Pd content in Pd@UiO-66-$NH_2$/R (3.55 wt%) is much higher than those obtained by $H_2$ reduction (2.12 wt%) and $NaBH_4$ reduction (2.35 wt%). Therefore, γ-radiation reduction stands out as a unique method to encapsulate ultrasmall metal NPs into MOFs due to the high penetrability of γ-rays and strong reduction capability of active species generated by γ-ray radiation.

The liquid-phase hydrogenation of olefins with different molecular sizes (1-hexene, trans-stilbene, and tetraphenylethylene) was carried out over Pd@UiO-66-$NH_2$/R and Pd/C to verify the size-selective catalysis of Pd@UiO-66-$NH_2$/R based on the fact that Pd NPs were confined in the UiO-66-$NH_2$ frameworks. As shown in Fig. 3, Pd@UiO-66-$NH_2$/R exhibits different conversion rates for olefins with different molecular sizes. For 1-hexene (2.5 Å), Pd@UiO-66-$NH_2$/R shows the highest activity with a 99.5% conversion rate after the 24 h reaction while the Pd/C catalyst exhibits a similar conversion rate (99.2%), indicating that there is no obvious difference between Pd@UiO-66-$NH_2$/R and Pd/C for the catalytic hydrogenation of small molecules. The reason is that the molecular size of 1-hexene is much smaller than the pore aperture of UiO-66-$NH_2$ (6 Å),[42] and thus the diffusion of 1-hexene is barely hindered by UiO-66-$NH_2$. trans-Stilbene has a much larger molecular size (5.6 Å) than 1-hexene and the conversion rate decreases to 83.2% using Pd@UiO-66-$NH_2$/R. In contrast, Pd/C displays a much lower conversion rate of 70.4%. Moreover, Pd@UiO-66-$NH_2$/R is not active toward the hydrogenation of tetraphenylethylene (6.7 Å), whereas Pd/C shows a moderate activity of 41.7% conversion rate (Fig. S7†). This is because tetraphenylethylene is too large to diffuse through the aperture of UiO-66-$NH_2$ and thus could not be catalysed by the Pd NPs confined inside the MOFs. The above results confirm that Pd NPs are confined inside the UiO-66-$NH_2$ frameworks.

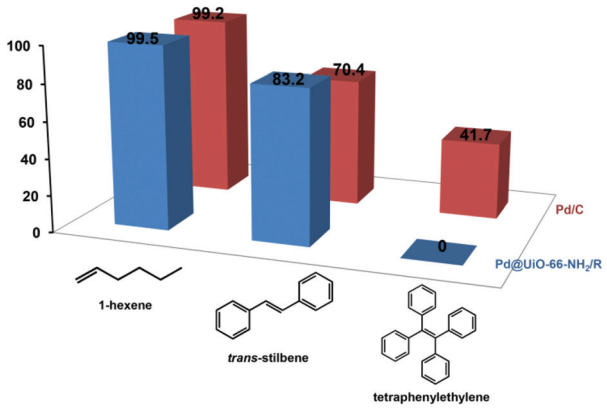


**Fig. 3** Catalytic performance of Pd@UiO-66-$NH_2$/R (3.55 wt% Pd) for the liquid-phase hydrogenation of olefins with different molecular sizes. The Pd/C catalyst (5 wt%) was used as a control.

Subsequently, the hydrogenation of styrene was performed over different heterogeneous Pd@UiO-66-$NH_2$ catalysts to evaluate the catalytic performance. As shown in Fig. 4a, under the given reaction conditions (the molar ratio of Pd to styrene was 1 : 100), Pd@UiO-66-$NH_2$/R exhibits the highest catalytic efficiency among different Pd@UiO-66-$NH_2$ catalysts. The hydrogenation of styrene using Pd@UiO-66-$NH_2$/R with Pd loading of 1.52 wt%, 3.55 wt% and 6.90 wt% could be completed (100% conversion) within 45 min, 50 min and 70 min, respectively, whereas Pd@UiO-66-$NH_2$/H and Pd@UiO-66-$NH_2$/B required 130 min and 140 min, respectively. The catalytic performance of Pd@UiO-66-$NH_2$/R was also superior to most of the reported Pd/MOF-based catalysts as shown in Table S5.† Meanwhile, pure UiO-66-$NH_2$ frameworks were not catalytically active toward the unsaturated olefin. These results suggest that the diameter, distribution, and surface-clean surface of Pd NPs could have a significant influence on the catalytic performance. 1.52 wt% Pd@UiO-66-$NH_2$/R is slightly more efficient than 3.55 wt% Pd@UiO-66-$NH_2$/R and 6.90 wt% Pd@UiO-66-$NH_2$/R owing to its smaller particle size as shown in Fig. S3.† Therefore, the high catalytic activity of Pd@UiO-66-$NH_2$/R could be attributed to the uniformly dispersed and highly active Pd NPs derived from γ-ray radiation. Furthermore, a hot-filtration experiment was conducted to investigate whether the reaction proceeded in a heterogeneous model. After the reaction proceeded for 20 min over different Pd@UiO-66-$NH_2$ catalysts, the solid catalysts were separated by hot-filtration and the filtrates were further maintained at the same temperature for additional 40 min. Obviously, the reaction was completely terminated after the removal of catalysts (Fig. S8†), suggesting that hydrogenation of styrene proceeds over the metal surface *via* a heterogeneous manner.

 This journal is © the Partner Organisations 2018

Published on 16 October 2017. Downloaded on 17/01/2018 00:24:45.

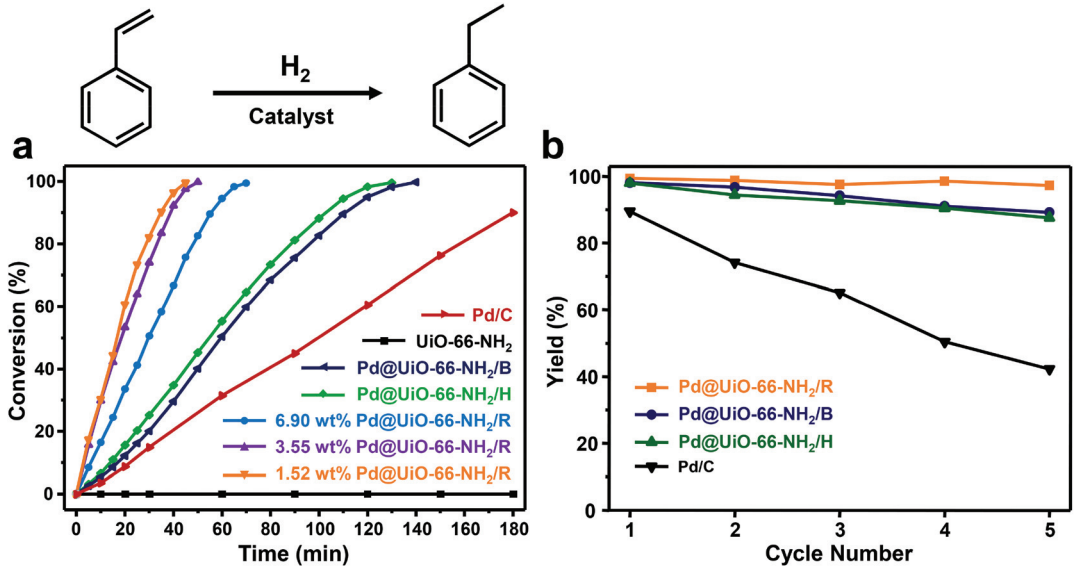


**Fig. 4** (a) Conversion of styrene as a function of the reaction time for Pd@UiO-66-$NH_2$ catalysts synthesized by different reduction methods (the molar ratio of Pd : styrene = 1 : 100). Pure UiO-66-$NH_2$ and Pd/C (5 wt%) were used as controls. (b) Durability and recyclability tests of different catalysts: Pd@UiO-66-$NH_2$/R (3.55 wt%), Pd@UiO-66-$NH_2$/H (2.12 wt%), Pd@UiO-66-$NH_2$/B (2.35 wt%), and Pd/C (5 wt%).

The stability of these heterogeneous catalysts was further evaluated for five consecutive catalytic cycles. As shown in Fig. 4b, the catalytic activity of Pd@UiO-66-$NH_2$/R remains almost the same for five cycles, whereas Pd@UiO-66-$NH_2$/H and Pd@UiO-66-$NH_2$/B exhibit gradual loss in catalytic performance after five cycles. We analysed the liquid phase of the reaction mixtures through hot-filtration after the first cycle by ICP-MS. It turned out that only 0.75 ppm of Pd leached out from Pd@UiO-66-$NH_2$/R, which was much lower than those observed in Pd@UiO-66-$NH_2$/H (6.06 ppm) and Pd@UiO-66-$NH_2$/B (6.07 ppm). Consequently, Pd@UiO-66-$NH_2$/R exhibited much enhanced stability during cycling tests. Meanwhile, detailed characterization using TEM indicated that no obvious aggregation could be observed in Pd@UiO-66-$NH_2$/R even after five consecutive tests (Fig. S4†). However, severe agglomeration of Pd nanoparticles can be observed in both Pd@UiO-66-$NH_2$/H and Pd@UiO-66-$NH_2$/B (Fig. S4†). More importantly, all samples were subjected to calcination at 250 °C under air for 2 h and only Pd NPs in Pd@UiO-66-$NH_2$/R still remained in the dispersed state. These results clearly reveal the excellent stability of Pd@UiO-66-$NH_2$/R due to the fact that γ-ray radiation could generate highly dispersed Pd NPs confined within the MOFs to avoid aggregation.

We also conducted X-ray diffraction and $N_2$ sorption measurements for the Pd@UiO-66-$NH_2$/R after cycling tests. The crystal structure of UiO-66-$NH_2$ still maintained after five cycles (Fig. S9†), and the BET surface area and the pore volume slightly decreased to 688 $m^2\ g^{-1}$ (Fig. S10†) and 0.29 $cm^3\ g^{-1}$ (Table S4†), respectively. The slight variation in the BET surface area and pore volume could be caused by the residual reactants or products trapped inside the Pd@UiO-66-$NH_2$/R.[32] Moreover, XPS analysis indicated that the $3d_{5/2}$ and $3d_{3/2}$ Pd peaks in Pd@UiO-66-$NH_2$/R remained unchanged after five cycles (Fig. S11†).

Furthermore, the catalytic reduction of 4-nitrophenol by $NaBH_4$ was also employed as a model reaction to evaluate the catalytic activity of Pd@UiO-66-$NH_2$ samples prepared using different methods. As shown in Fig. S12–S15,† it is obvious that the intensity of the characteristic absorption peak of 4-nitrophenol at 400 nm decreases quickly in the presence of catalysts and the characteristic absorption of 4-aminophenol at ~305 nm appears and gradually increases with reaction time. The reduction of 4-nitrophenol completed in 355 s after adding Pd@UiO-66-$NH_2$/R (Fig. S12†). In contrast, the reaction took much longer time to complete when Pd@UiO-66-$NH_2$/H (580 s), Pd@UiO-66-$NH_2$/B (640 s) and Pd/C (860 s) were used as the catalyst. Moreover, according to the slope of the fitted line plotted with $\ln(C_t/C_0)$ *versus* the reaction time (Fig. 5), the kinetic constant $k_{app}$ for the reduction of 4-nitrophenol over Pd@UiO-66-$NH_2$/R was 0.02425 $s^{-1}$ (1.455 $min^{-1}$) which is much higher than those obtained in Pd@UiO-66-$NH_2$/B (1.126 $min^{-1}$), Pd@UiO-66-$NH_2$/H (1.123 $min^{-1}$) and Pd/C (0.341 $min^{-1}$). This value is also much better than other Pd-based catalysts (Table S6†), implying that γ-ray radiation is a powerful tool to prepare ultrasmall Pd NPs with excellent catalytic performance.

Our study demonstrates that γ-ray radiation reduction is a facile and efficient approach to *in situ* generate Pd NPs inside UiO-66-$NH_2$. This approach could also be extended to encapsulate other metal NPs into UiO-66-$NH_2$. For example, we used the same strategy to successfully obtain highly dispersed Pt and Au NPs inside UiO-66-$NH_2$ frameworks. As shown in Fig. 6a and b, TEM images clearly reveal that highly dispersed Pt and Au NPs with an average diameter of ~1.0 nm are encap-

Published on 16 October 2017. Downloaded on 17/01/2018 00:24:45.

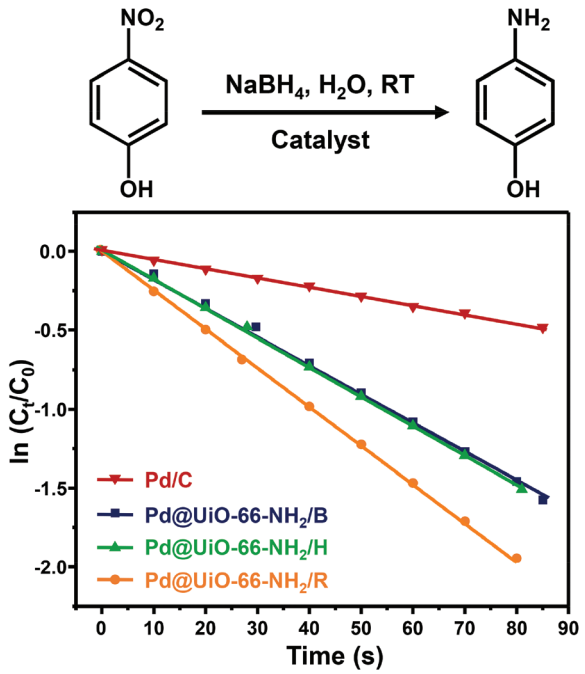


**Fig. 5** Plots of $\ln(C_t/C_0)$ at 400 nm *versus* the reaction time for Pd@UiO-66-$NH_2$ synthesized by different reduction methods and Pd/C (5 wt%) as a control (molar ratio of Pd : 4-nitrophenol = 1 : 150).

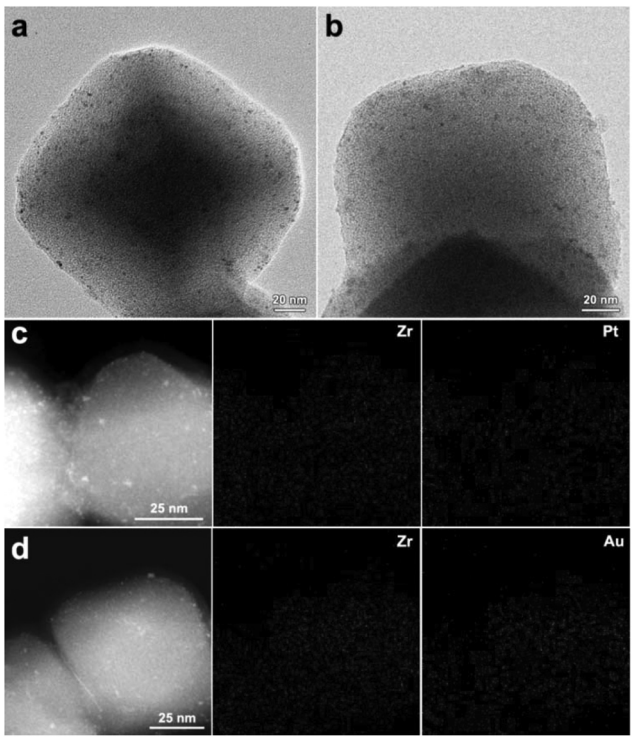


**Fig. 6** TEM images of (a) Pt@UiO-66-$NH_2$/R and (b) Au@UiO-66-$NH_2$/R synthesized through the γ-ray radiation method. HAADF-STEM images of (c) Pt@UiO-66-$NH_2$/R and (d) Au@UiO-66-$NH_2$/R and their corresponding elemental mapping images.

sulated inside the UiO-66-$NH_2$ frameworks. The corresponding elemental mapping images further indicate that Pt and Au are evenly dispersed within UiO-66-$NH_2$ (Fig. 6c and d). Furthermore, the structural integrity of UiO-66-$NH_2$ could be maintained in both Pt@UiO-66-$NH_2$/R and Au@UiO-66-$NH_2$/R and no detectable diffraction peaks of Pt and Au were observed (Fig. S16†). The nitrogen sorption isotherms of Pt@UiO-66-$NH_2$/R and Au@UiO-66-$NH_2$/R exhibited the similar features to those of Pd@UiO-66-$NH_2$/R (Fig. S17†). Furthermore, γ-ray radiation reduction also works well in generating metal NPs *in situ* inside other MOFs. Fig. S18† shows Pd@MIL-101/R and Pt@MIL-101/R as examples. Therefore, the newly developed γ-ray radiation approach is very versatile for the synthesis of highly active metal NPs inside MOFs with excellent stability and catalytic performance.

## 4. Conclusions

In conclusion, we have successfully demonstrated a novel γ-ray radiation approach for the synthesis of highly dispersed Pd NPs with uniform sizes inside MOFs. The confined Pd NPs in Pd@UiO-66-$NH_2$/R exhibited enhanced catalytic performance and improved stability in olefin hydrogenation and catalytic reduction of 4-nitrophenol compared to Pd@UiO-66-$NH_2$/H and Pd@UiO-66-$NH_2$/B, indicating that the surface-clean metal NPs generated inside MOFs using this approach are very promising for catalytic applications. Our study also reveals that this γ-ray radiation method is more efficient in converting metal ions into catalytically active metal species. Considering that the radiation technique is widely used in industry, this approach could potentially produce other MOF composites in a scalable manner. Studies aimed at extending this methodology to encapsulate other catalytic species into MOFs for more intriguing catalytic applications are currently underway in our laboratory.

## Conflicts of interest

There are no conflicts to declare.

## Acknowledgements

We acknowledge the funding support from MOST (2015CB351903, 2017YFA0207301, and 2014CB931803), National Natural Science Foundation of China (51402282, 51373160, 21474095, 21371162, 21673213, and 21521001), CAS Key Research Program of Frontier Sciences (QYZDB-SSW-SLH018), and the Fundamental Research Funds for the Central Universities.

## References

1 Y. J. Colón and R. Q. Snurr, *Chem. Soc. Rev.*, 2014, **43**, 5735–5749.

 This journal is © the Partner Organisations 2018

Published on 16 October 2017. Downloaded on 17/01/2018 00:24:45.

2 W. Zhang, Y. Liu, G. Lu, Y. Wang, S. Li, C. Cui, J. Wu, Z. Xu, D. Tian, W. Huang, J. S. Ducheneu, W. D. Wei, H. Chen, Y. Yang and F. W. Huo, *Adv. Mater.*, 2015, **27**, 2923–2929.
3 W. Lu, Z. Wei, Z.-Y. Gu, T.-F. Liu, J. Park, J. Park, J. Tian, M. Zhang, Q. Zhang, T. Gentle III, M. Bosch and H.-C. Zhou, *Chem. Soc. Rev.*, 2014, **43**, 5561–5593.
4 J. K. Guo, K. Q. Ye, M. He, W.-W. Xiong, W. F. Cao, Z. Y. Lee, Y. Wang, T. Wu, F. W. Huo, X. G. Liu and Q. C. Zhang, *J. Solid State Chem.*, 2013, **206**, 27–31.
5 J. Zhao, Y. N. Wang, W. W. Dong, Y. P. Wu, D. S. Li, B. Liu and Q. C. Zhang, *Chem. Commun.*, 2015, **51**, 9479–9482.
6 J. R. Li, J. Sculley and H.-C. Zhou, *Chem. Rev.*, 2012, **112**, 869–932.
7 X. Cui, K. Chen, H. Xing, Q. Yang, R. Krishna, Z. Bao, H. Wu, W. Zhou, X. Dong, Y. Han, B. Li, Q. Ren, M. J. Zaworotko and B. L. Chen, *Science*, 2016, **353**, 141–144.
8 A. Cadiau, K. Adil, P. M. Bhatt, Y. Belmabkhout and M. Eddaoudi, *Science*, 2016, **353**, 137–140.
9 T. A. Makal, J.-R. Li, W. Lu and H.-C. Zhou, *Chem. Soc. Rev.*, 2012, **41**, 7761–7779.
10 S. Chaemchuen, N. A. Kabir, K. Zhou and F. Verpoort, *Chem. Soc. Rev.*, 2013, **42**, 9304–9332.
11 L.-B. Sun, A.-G. Li, X.-D. Liu, X.-Q. Liu, D. Feng, W. Lu, D. Yuan and H.-C. Zhou, *J. Mater. Chem. A*, 2015, **3**, 3252–3256.
12 L. E. Kreno, K. Leong, O. K. Farha, M. Allendorf, R. P. Van Duyne and J. T. Hupp, *Chem. Rev.*, 2012, **112**, 1105–1125.
13 Z. Hu, B. J. Deibert and J. Li, *Chem. Soc. Rev.*, 2014, **43**, 5815–5840.
14 M. D. Allendorf, C. A. Bauer, R. K. Bhakta and R. J. T. Houk, *Chem. Soc. Rev.*, 2009, **38**, 1330–1352.
15 J. Della Rocca, D. Liu and W. Lin, *Acc. Chem. Res.*, 2011, **44**, 957–968.
16 P. Horcajada, R. Gref, T. Baati, P. K. Allan, G. Maurin, P. Couvreur, G. Férey, R. E. Morris and C. Serre, *Chem. Rev.*, 2012, **112**, 1232–1268.
17 Q. H. Yang, Q. Xu, S.-H. Yu and H.-L. Jiang, *Angew. Chem., Int. Ed.*, 2016, **55**, 3685–3689.
18 A. Dhakshinamoorthy and H. Garcia, *Chem. Soc. Rev.*, 2014, **43**, 5750–5765.
19 Q. H. Yang, Q. Xu and H.-L. Jiang, *Chem. Soc. Rev.*, 2017, **46**, 4774–4808.
20 X.-Q. Wu, D.-D. Huang, Z.-H. Zhou, W.-W. Dong, Y.-P. Wu, J. Zhao, D.-S. Li, Q. C. Zhang and X. H. Buc, *Dalton Trans.*, 2017, **46**, 2430–2438.
21 G.-W. Xu, Y.-P. Wu, W.-W. Dong, J. Zhao, X.-Q. Wu, D.-S. Li and Q. C. Zhang, *Small*, 2017, **13**, 1602996.
22 P. Valvekens, F. Vermoortele and D. De Vos, *Catal. Sci. Technol.*, 2013, **3**, 1435–1445.
23 M. Yoon, R. Srirambalaji and K. Kim, *Chem. Rev.*, 2012, **112**, 1196–1231.
24 A. Dhakshinamoorthy, *Chem. Soc. Rev.*, 2012, **41**, 5262–5284.
25 L.-B. Sun, X.-Q. Liu and H.-C. Zhou, *Chem. Soc. Rev.*, 2015, **44**, 5092–5147.
26 S. Li and F. W. Huo, *Nanoscale*, 2015, **7**, 7482–7501.
27 Q.-L. Zhu and Q. Xu, *Chem*, 2016, **1**, 220–245.
28 W. Zhou, B. Zou, W. Zhang, D. Tian, W. Huang and F. W. Huo, *Nanoscale*, 2015, **7**, 8720–8724.
29 G. Huang, Q. H. Yang, Q. Xu, S.-H. Yu and H.-L. Jiang, *Angew. Chem., Int. Ed.*, 2016, **55**, 7379–7383.
30 I. Luz, C. Rösler, K. Epp, F. X. LlabresiXamena and R. A. Fischer, *Eur. J. Inorg. Chem.*, 2015, **32**, 3904–3912.
31 A. Aijaz, A. Karkamkar, Y. J. Choi, N. Tsumori, E. Rönnebro, T. Autrey, H. Shioyama and Q. Xu, *J. Am. Chem. Soc.*, 2012, **134**, 13926–13929.
32 X. Li, Z. Guo, C. Xiao, T. W. Goh, D. Tesfagaber and W. Y. Huang, *ACS Catal.*, 2014, **4**, 3490–3497.
33 Z. Guo, C. Xiao, R. V. Maligal-Ganesh, L. Zhou, T. W. Goh, X. Li, D. Tesfagaber, A. Thiel and W. Y. Huang, *ACS Catal.*, 2014, **4**, 1340–1348.
34 H. Liu, L. Chang, C. Bai, L. Chen, R. Luque and Y. W. Li, *Angew. Chem., Int. Ed.*, 2016, **55**, 5019–5023.
35 Y. F. Yang, F. W. Wang, Q. H. Yang, Y. L. Hu, H. Yan, Y. Z. Chen, H. R. Liu, G. Q. Zhang, J. L. Lu, H.-L. Jiang and H. X. Xu, *ACS Appl. Mater. Interfaces*, 2014, **6**, 18163–18171.
36 M. Zhao, K. Deng, L. He, Y. Liu, G. Li, H. J. Zhao and Z. Y. Tang, *J. Am. Chem. Soc.*, 2014, **136**, 1738–1741.
37 C. Kuo, Y. Tang, L. Chou, B. T. Sneed, C. N. Brodsky, Z. Zhao and C.-K. Tsung, *J. Am. Chem. Soc.*, 2012, **134**, 14345–14348.
38 P. Wang, J. Zhao, X. Li, Y. Yang, Q. Yang and C. Li, *Chem. Commun.*, 2013, **49**, 3330–3332.
39 T. Tsuruoka, H. Kawasaki, H. Nawafuneand and K. Akamatsu, *ACS Appl. Mater. Interfaces*, 2011, **3**, 3788–3791.
40 H. L. Liu, L. Chang, L. Chen and Y. W. Li, *J. Mater. Chem. A*, 2015, **3**, 8028–8033.
41 W. Dong, C. Feng, L. Zhang, N. Shang, S. Gao, C. Wang and Z. Wang, *Catal. Lett.*, 2016, **146**, 117–125.
42 C. Liang, W. Xia, H. Soltani-Ahmadi, O. Schluter, R. A. Fischer and M. Muhler, *Chem. Commun.*, 2005, **2**, 282–284.
43 C. Dispenza, N. Grimaldi, M. A. Sabatino, I. L. Soroka and M. Jonsson, *J. Nanosci. Nanotechnol.*, 2015, **15**, 3445–3467.
44 H. R. Liu, X. W. Ge, X. Xu, Z. C. Zhang and M. W. Zhang, *Radiat. Phys. Chem.*, 1999, **55**, 357–361.
45 Y. J. Zhang, Y. T. Qian, M. W. Zhang, Z. Y. Chen, B. Lu and C. S. Wang, *Mater. Lett.*, 1993, **17**, 314–318.
46 L. He, L. F. Dumée, D. Liu, L. Velleman, F. She, C. Banos, J. B. Davies and L. Kong, *RSC Adv.*, 2015, **5**, 10707–10715.
47 J. L. Marignier, J. Belloni, M. O. Delcourt and J. P. Chevalier, *Nature*, 1985, **317**, 344–345.
48 P. Yadav, R. T. Olsson and M. Jonsson, *Radiat. Phys. Chem.*, 2009, **78**, 939–944.
49 L. M. Alrehaily, J. M. Joseph, M. C. Biesinger, D. A. Guzonas and J. C. Wren, *Phys. Chem. Chem. Phys.*, 2013, **15**, 1014–1024.
50 Y. P. Liu, Y. Zhang, M. W. Zhang, W. Zhang, Y. T. Qian, L. Yang, C. Wang and Z. Chen, *Mater. Sci. Eng., B*, 1997, **49**, 42–45.

51 P. A. Yakabuskie, J. M. Joseph, P. Keech, G. A. Botton, D. Guzonas and J. C. Wren, *Phys. Chem. Chem. Phys.*, 2011, **13**, 7198–7206.
52 H. S. Bae, E. H. Shim, J. Hoon Park and H. Jung, *J. Phys. Chem. Solids*, 2012, **73**, 1456–1459.
53 S. W. Kim, B. J. Kwon, J. H. Park, M. G. Hur, S. D. Yang and H. Jung, *Bull. Korean Chem. Soc.*, 2010, **31**, 910–914.
54 A. Kharazmi, E. Saion, N. Faraji, N. Soltani and A. Dehzangi, *Chin. Phys. Lett.*, 2013, **30**, 057803–057807.
55 A. K. Sahoo, S. K. Srivastava, P. K. Raul, A. K. Gupta and R. Shrivastava, *J. Nanopart. Res.*, 2014, **16**, 2473–2489.
56 Y. D. Yin, X. Xu, X. W. Ge, Y. Lu and Z. C. Zhang, *Radiat. Phys. Chem.*, 1999, **55**, 353–356.
57 Y. D. Yin, X. Xu and Z. C. Zhang, *Chem. Commun.*, 1998, **16**, 1641–1642.
58 S. H. Choi, Y. P. Zhang, A. Gopalan, K. P. Lee and H. D. Kang, *Colloids Surf., A*, 2005, **256**, 165–170.
59 J. H. Cavka, S. Jakobsen, U. Olsbye, N. Guillou, C. Lamberti, S. Bordiga and K. P. Lillerud, *J. Am. Chem. Soc.*, 2008, **130**, 13850–13851.
60 J. V. Rojas and C. H. Castano, *Radiat. Phys. Chem.*, 2012, **81**, 16–21.
61 X. Li, T. W. Goh, L. Li, C. Xiao, Z. Guo, X. C. Zeng and W. Y. Huang, *ACS Catal.*, 2016, **6**, 3461–3468.
62 L. Chen, H. Chen, R. Luque and Y. Li, *Chem. Sci.*, 2014, **5**, 3708–3714.
63 R. Kardanpour, S. Tangestaninejad, V. Mirkhani, M. Moghadam, I. Mohammadpoor-Baltork, A. R. Khosropour and F. Zadehahmadi, *J. Organomet. Chem.*, 2014, **761**, 127–133.

Published on 16 October 2017. Downloaded on 17/01/2018 00:24:45.


This journal is © the Partner Organisations 2018